Ultraprecise age and formation temperature of the Australasian tektites constrained by 40 Ar/ 39 Ar analyses

Frederic Jourdan, Sebastien Nomade, Michael T. D. Wingate, Ela Eroglu, Alan Deino

The Meteoritical Society

Meteoritics & Planetary Science 54, Nr 10, 2573–2591 (2019)
doi: 10.1111/maps.13305

Ultraprecise age and formation temperature of the Australasian tektites constrained by $^{40}Ar/^{39}Ar$ analyses

Fred JOURDAN[1*], Sebastien NOMADE[2], Michael T. D. WINGATE[3], Ela EROGLU[4], and Al DEINO[5]

[1]Western Australian Argon Isotope Facility, JdL Centre & School of Earth and Planetary Sciences, Curtin University, GPO Box U1987, Perth, Western Australia 6845, Australia
[2]Laboratoire des Sciences du Climat et de L'Environnement, UMR 8212, LSCE/IPSL, CEA-CNRS-UVSQ, Université Paris-Saclay, Gif-Sur-Yvette, France
[3]Dept of Mines, Industry Regulation and Safety, Geological Survey of Western Australia, East Perth, Western Australia 6004, Australia
[4]Department of Chemical Engineering, Curtin University, Perth, Western Australia 6845, Australia
[5]Berkeley Geochronology Center, 2455 Ridge Rd., Berkeley, California 94709, USA
[*]Corresponding author. E-mail: f.jourdan@curtin.edu.au

(Received 24 August 2018; revision accepted 25 April 2019)

Abstract–The Australasian tektites are quench melt glass ejecta particles distributed over the Asian, Australian, and Antarctic regions, the source crater of which is currently elusive. New $^{40}Ar/^{39}Ar$ age data from four tektites: one each from Thailand, China, Vietnam, and Australia measured using three different instruments from two different laboratories and combined with published $^{40}Ar/^{39}Ar$ data yield a weighted mean age of 788.1 ± 2.8 ka (±3.0 ka, including all sources of uncertainties) (P = 0.54). This age is five times more precise compared to previous results thanks, in part, to the multicollection capabilities of the ARGUS VI noble gas mass spectrometer, which allows an improvement of almost fourfold on a single plateau age measurement. Diffusion experiments on tektites combined with synthetic age spectra and Monte Carlo diffusion models suggest that the minimum temperature of formation of the Thai tektite is between 2350 °C and 3950 °C, hence a *strict minimum* value of 2350 °C.

INTRODUCTION

The Australasian tektites and microtektites are quench melt glass ejecta particles distributed over the Southeastern Asian, Australian, and Antarctic regions and cover about 20% of Earth's surface (Folco et al. 2009; Schwarz et al. 2016). Because all Australasian tektites yield similar isotopic ages around 0.8 Ma, they are considered the product of a single hypervelocity impact, for which source crater is currently unknown, but is probably located in the Indochina region, although estimates vary (Glass and Koeberl 2006; Mizera et al. 2016; Cavosie et al. 2018).

Tektites are composed of K-bearing glass, with most containing a very small amount of undigested clasts, and therefore are a prime candidate for $^{40}Ar/^{39}Ar$ dating. Nevertheless, precise dating of quaternary impact events is notoriously difficult due to inherent problems in dating young impact glass material. This case is well illustrated by only four quaternary impact events (over ~32 confirmed quaternary impact structures) dated by the $^{40}Ar/^{39}Ar$ technique, with ages of 570 ± 47 ka (2σ[1]; ±8%) obtained for the Lonar crater melt rock (Jourdan et al. 2011), 1.10 ± 0.05 Ma (±4.5%) obtained for Ivory Coast (Bosumtwi crater) tektites (Koeberl et al. 1997), 1.57 ± 0.14 Ma (±9%) obtained for the Tenoumer crater melt rock (Schultze et al. 2016), and 793 ± 14 ka (±1.8%) determined for Australasian tektites by Schwarz et al. (2016). Furthermore, the range of time–temperature (*T*–*t*) regimes undergone by tektites at the time of their formation is currently based on a minimum temperature

[1]All ages in this study are indicated at 2σ.

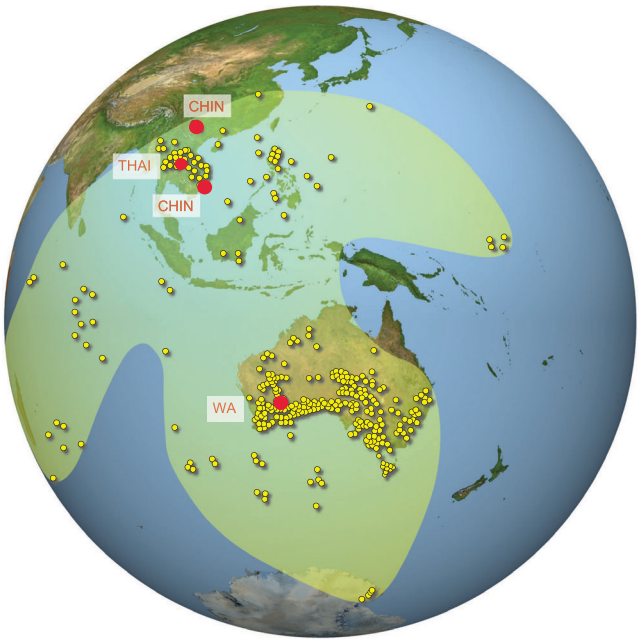

Fig. 1. The Australasian tektite strewn field after Folco et al. (2009). Western Canada has been reported to contain Australasian tektites that could result from ballistic transport. However, it still remains to be confirmed that they were not brought by humans (Schwarz et al. 2016), hence are not included in this map at this stage. (Color figure can be viewed at wileyonlinelibrary.com.)

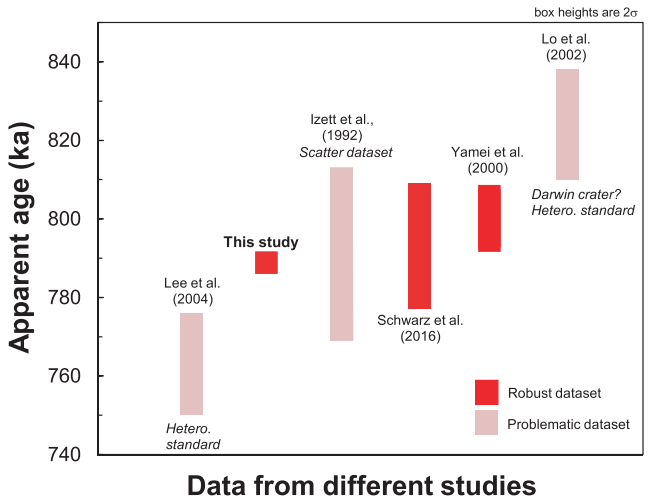

Fig. 2. Apparent $^{40}Ar/^{39}Ar$ ages (incorporating 2σ uncertainties) obtained by various studies (cf. text). Ages using heterogeneous standards for age calculations (Lo et al. 2002; Lee et al. 2004) or using statistically discordant data set (Izett and Obrandovich 1992) are indicated using a lighter fill. The most robust ages are indicated with a darker fill (Yamei et al. 2000; Schwarz et al. 2016; this study). All ages have been recalculated using the constants of Renne et al. (2011). Hetero. = heterogeneous. (Color figure can be viewed at wile yonlinelibrary.com.)

of 1673 °C derived from the presence of former reidite reverted to zircon found in an Australasian Muong Nong-type tektite from Thailand (Cavosie et al. 2018).

In this study, we conducted eight $^{40}Ar/^{39}Ar$ step-heating age analyses on four tektites: one each from Australia, China, Vietnam, and Thailand, using three different mass spectrometers (ARGUS VI, MAP-215-50, and VG5400) in two different laboratories. Our goal was to improve the accuracy and precision of the formation age of the tektites. Deriving the most precise and accurate age for the formation of Australasian tektites is important not only for impact crater research but also for stratigraphic age correlation used in climate research (e.g., Mark et al. 2017). We also conducted additional diffusion experiments to quantify the diffusion characteristics of each tektite and combine those results with diffusion models to elucidate the *T*–*t* history experienced by the tektites.

Australasian Tektites and Their Ages

The Australasian tektites and microtektites are found over a wide area, including southeast Asia, Australia, and Antarctica (Fig. 1; e.g., Folco et al. 2009). Their chemical composition varies between a well-defined range of values, and is partially correlated with the location where they have been found (Folco et al. 2010; Schwarz et al. 2016). All the tektites are easily differentiated from volcanic glass by their very low water concentrations (Beran and Koeberl 1997).

Over the last three decades, several $^{40}Ar/^{39}Ar$ laboratories have analyzed Australasian tektites from various locations and agree on an age of approximately 0.8 Ma. In detail, however, those ages are not all in agreement (Jourdan 2012). All ages in this study were recalibrated or directly calculated using the ^{40}K decay constants and standard ages of Renne et al. (2011), except for the ACs standard where we used the most recent R-value calibration of Niespolo et al. (2017). The recalculated ages (Fig. 2) ranged from 763 ± 13 ka (Lee et al. 2004) to 800 ± 6 ka (Yamei et al. 2000). In addition, impact glass ejecta from western Tasmania, known as "Darwin glass," which has a disputed origin as either part of the Australasian tektites or the putative Tasmanian Darwin crater ejecta suite, yielded a $^{40}Ar/^{39}Ar$ age of 824 ± 15 ka (Lo et al. 2002).

Previous $^{40}Ar/^{39}Ar$ Geochronology

Total Fusion Analyses

Previous measurements have been carried out using different approaches with mixed results. One approach is total fusion analysis, in which glass particles are fused in a single step. Izett and Obrandovich (1992) used this technique on glass samples but obtained a set of data

that showed significant statistical scatter (MSWD = 3.06), likely due to either inherited radiogenic ^{40}Ar ($^{40}Ar^*$) not fully degassed upon impact (Jourdan et al. 2007) or $^{40}Ar^*$ loss, and thus, an unreliable apparent age was derived from the error-chron (see discussion on the importance of data concordance in age accurate determination in Jourdan 2012; Jourdan et al. 2009, 2012). Lo et al. (2002) used a similar approach, except they measured a series of single glass fragments for each of three tektites and obtained concordant results. These authors pooled the resulting analyses for all three tektites and obtained a (recalculated) age of 824 ± 15 ka, with a P-value of 0.075 (MSWD = 1.2, n = 108). This result appears robust, but the question remains whether it dates the formation of the putative Darwin crater in Tasmania (i.e., Darwin glass) or the formation of Australasian tektites that happened to land in Tasmania. Furthermore, an important caveat is that these authors used the LP-6 biotite standard which has been shown to consist of a binary mixture between two different age components with ages of 120 and 135 Ma (Roddick 1983), and as a result, its use has been strongly discouraged (Baksi et al. 1996; Spell and McDougall 2003; Jourdan and Renne 2007). Lee et al. (2004) carried out analyses in the same laboratory using the same analytical conditions and LP-6 standards as Lo et al. (2002) and obtained an apparent (recalculated) age of 763 ± 13 ka (P = 1.0; recalculated). This age is significantly different from the age obtained on the Darwin glass suggesting either that the Darwin crater is a true impact crater and formed earlier than the Australasian tektites or that the apparent age variation in Australasian tektites was caused by use of the heterogeneous LP-6 standard. Regardless, we consider that the use of the LP-6 standards makes the two latter results unreliable for precise age calculations.

Step-Heating Analyses

Yamei et al. (2000) carried out step-heating analyses on multiple replicates from three different tektites from the Bose site in China, and obtained a series of plateau and isochron ages with a recalculated mean age of 800 ± 6 ka. However, Mark et al. (2017) suggested that the isochron plot indicates that those data are affected by minor excess ^{40}Ar and are thus slightly too old as shown by the lack of compatibility with the precise time scale determined by Mark et al. (2017) using Toba ash bed products (cf. discussion below).

More recently, Schwarz et al. (2016) analyzed aliquots from eight tektites using a furnace step-heating approach with almost all analyses yielding plateau ages, and with the plateau being corrected from non-atmospheric trapped $^{40}Ar/^{36}Ar$ using a bulk isochron intercept for some tektites. They calculated a weighted mean age of 793 ± 16 ka (P = 1.0, recalculated) for the Australasian tektites, suggesting very homogenous data and thus a robust age. If a western Canadian tektite (suspected to be an Australasian tektite brought by humans to North America or alternatively, transported directly to North America through ballistic flight) is included in the calculation, the age gets slightly more precise at 793 ± 14 ka (Schwarz et al. 2016).

METHODOLOGY

We prepared multiple aliquots from four different tektites: one each from Western Australia (diameter [d] ~1.5 cm; found on a salt lake 137 km SE of Kalgoorlie), China (d ~1.5 cm; collected in the Bose basin, Guangxi Zhuang region with details given by Yamei et al. 2000), Thailand (d ~1 cm; Nakhon Ratahasina town district), and Vietnam (d ~0.8 cm; Bảo Lộc, Lâm Đồng, northeast of Ho Chi Minh Ville) (Fig. 1 and Table 1). All tektites used in this study classify as splash form with spherical to subspherical appearances and consist of the whole tektite.

Analyses at the Western Australian Argon Isotope Facility, Curtin University

We prepared eight fresh separates from the four different tektites (i.e., two separates per tektite) mentioned above for $^{40}Ar/^{39}Ar$ dating. Fresh tektite fragments, 300–400 μm in size, were carefully handpicked under a binocular microscope with a total weight of approximately 400 mg of picked material for each tektite. The glass fragments were thoroughly rinsed with distilled water in an ultrasonic cleaner. Samples were loaded into large wells of one 1.9 cm diameter and 0.3 cm depth aluminum disk. These wells were bracketed by small wells that included Fish Canyon sanidine (FCs) used as a neutron fluence monitor for which an age of 28.294 ± 0.036 Ma (1σ) was adopted (Renne et al. 2011). The disks were Cd-shielded (to minimize undesirable nuclear interference reactions) and irradiated during one of the two different irradiations for 3 h in the USGS TRIGA reactor, in Denver, Colorado (USA) or in the Oregon State University TRIGA reactor, in Corvallis, Oregon (USA). The mean J-values computed from standard grains within the small pits and determined as the average and standard deviation of J-values of the small wells for each irradiation disk are given along with the raw data in supporting information Annex S1. Mass discrimination is given in Annex S1 for each sample and was monitored using an automated air pipette and calculated relative to an air ratio of 298.56 ± 0.31 (Lee et al. 2006). Correction factors for interfering isotopes

Table 1. Summary table of $^{40}Ar/^{39}Ar$ data for 11 aliquots from four different tektites, showing plateau and inverse isochron characteristics. Approximate original size prior to sample preparation is indicated for all four tektites.

		General characteristics				Plateau characteristics					Isochron characteristics					
Sample	Initial diameter (cm)	Aliquot #	Region of provenance	Instrument used	Extraction system	Plateau age (ka; 2σ)	Total ^{39}Ar released (%)	Attribute	MSWD	P	Isochron age (Ma; 2σ)	n	$^{40}Ar/^{36}Ar$ intercept (Ma; 2σ)	MSWD	P	Spreading factor (%)[c]
Chin	~1.5cm	Chin-1	Bose (China)	ARGUS VI	Laser	792.1 ± 6.0	94%	P	0.8	0.67	795 ± 8	15	295 ± 7	0.8	0.66	50%
		Chin-2	Bose (China)	VG5400	Laser	790 ± 19	100%	P	0.1	1.00	791 ± 30	7	294 ± 44	0.04	0.99	
		Chin-3	Bose (China)	MAP215-50	Furnace		N/A[a]						N/A[a]			
Thai	~1 cm	Thai-1	Thailand	ARGUS VI	Laser	785.0 ± 4.4	96%	P	1.2	0.27	784.2 ± 5.5	15	299.4 ± 3.2	1.3	0.22	62%
		Thai-2	Thailand	VG5400	Laser	784 ± 15	100%	P	0.2	0.98	798 ± 28	7	264 ± 92			
		Thai-3	Thailand	MAP215-50	Furnace		N/A[a]						N/A[a]			
Viet	~0.8 cm	Viet-1	Vietnam	ARGUS VI	Laser	786.9 ± 6.0	79%	P	1.5	0.14	787.1 ± 7.2	13	297.0 ± 1.5	1.8	0.05	63%
		Viet-2	Vietnam	VG5400	Laser	788 ± 19	100%	P	0.1	0.98	810 ± 110	5	302 ± 160			
		Viet-3	Vietnam	MAP215-50	Furnace		N/A[a]						N/A[a]			
WA	~1.5 cm	WA-1	Western Australia	MAP 215-50	Furnace	795 ± 14	100%	P	0.4	0.98	806 ± 24	13	288 ± 20	0.4	0.97	28%
		WA-2	Western Australia	MAP 215-50	Furnace	797 ± 15	100%	P	0.6	0.82	792 ± 19	13	304 ± 16	0.7	0.75	54%
		Weighted mean all tektites (this study only; n = 8)				787.9 ± 2.8	[3.0][b]		0.9	0.48	789.0 ± 3.4	[3.6][b]		2.2	0.06	
		Weighted mean all tektites (this study & Schwarz et al. 2016, n = 9)				**788 ± 2.8**	**[3.0][b]**		0.9	0.54						

[a]Not available as all the reactor induced ^{37}Ar had already decayed at time of analysis preventing age calculation.
[b]All uncertainties included. Age in bold: preferred formation age of the Australasian tektites.
[c]Spreading factor calculated following Jourdan et al. (2009).

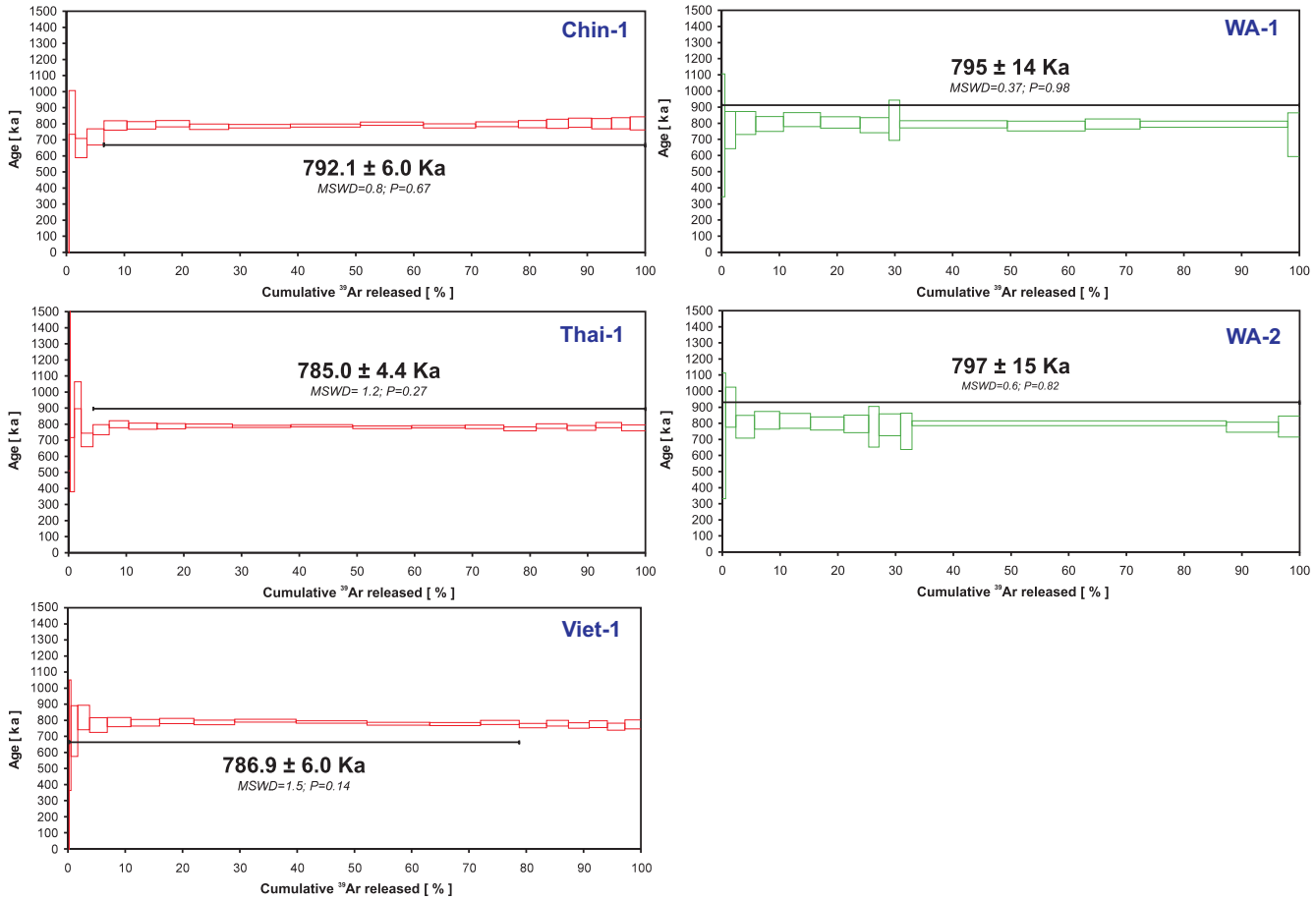

Fig. 3. $^{40}Ar/^{39}Ar$ apparent ages obtained at Curtin University with an ARGUS VI multicollector (red spectra) and a MAP 250-50 single collector (green spectra) instrument for a total of five aliquots from four tektites (Chinese, Thai, Vietnamese, and Western Australia). Plateau ages are quoted at the 2σ level. (Color figure can be viewed at wileyonlinelibrary.com.)

were $(^{39}Ar/^{37}Ar)_{Ca} = 7.06 \times 10^{-4}$ (±7%), $(^{36}Ar/^{37}Ar)_{Ca} = 2.81 \times 10^{-4}$ (±3%), and $(^{40}Ar/^{39}Ar)_{K} = 6.76 \times 10^{-4}$ (±10%) (Cosca et al. 2011) for the USGS TRIGA reactor and $(^{39}Ar/^{37}Ar)_{Ca} = 6.95 \times 10^{-4}$ (±1.3%), $(^{36}Ar/^{37}Ar)_{Ca} = 2.65 \times 10^{-4}$ (± 0.84%), and $(^{40}Ar/^{39}Ar)_{K} = 7.30 \times 10^{-4}$ (±12.4%) (Renne et al. 2013) for the OSU reactor. The $^{40}Ar/^{39}Ar$ analyses were performed at the Western Australian Argon Isotope Facility at Curtin University on two different instruments (either a MAP 215-50 or an ARGUS VI), for which details are provided below. The raw data were processed using the ArArCALC software (Koppers 2002) and ages were calculated using decay constants recommended by Renne et al. (2011). All parameters and relative abundance values are provided in individual supporting information Annexes and have been corrected for blank, mass discrimination, and radioactive decay.

Our criteria for the determination of plateaus are as follows: plateaus must include at least 70% of ^{39}Ar and be distributed over a minimum of three consecutive steps agreeing at 95% confidence levels and indicate a probability of fit (P) of at least 0.05. Plateau ages (Table 1 and Fig. 3) are given at the 2σ level and are calculated using the mean of all plateau steps, weighted by the inverse variances of their individual analytical uncertainties. Inverse isochrons include the maximum number of steps with a probability of fit ≥0.05. S-factors showing the spread along the inverse isochron (Jourdan et al. 2009) and $^{40}Ar/^{36}Ar$ intercept values are provided (Table 1). Uncertainties include analytical and J-value errors; those that incorporate all sources of uncertainty are indicated by square brackets (e.g., [±3.0 ka]). Finally, all ages given throughout the text from literature or calculated in this study are all given at the 2σ level.

Map 215-50

Two aliquots (~130 mg each; WA-1 and WA-2) from a large Australian tektite were step-heated within a temperature range of 500–1450 °C for 10 min (followed by rapid cooling to avoid subsequent gas loss) in a double-vacuum high-frequency Pond Engineering©

furnace for geochronology and diffusion parameter measurements. In addition, a total of three aliquots from the Vietnamese (Viet-3), Chinese (Chin-3), and Thai (Thai-3) tektites were analyzed with the MAP 215-50 instrument. The results were used to calculate diffusion parameters of the Ar in glass (i.e., "closure temperature") using ^{39}Ar as diffusant and an Arrhenius regression approach (Schmieder and Jourdan 2013). Unfortunately, the diffusion analyses were not suitable for deriving an age because all the ^{37}Ar produced during irradiation had already decayed at the time of the analyses. The gas was purified in a stainless steel extraction line using two AP10 and one GP50 SAES getters and a liquid nitrogen condensation trap for 10 min. Ar isotopes were measured in static mode using a MAP 215-50 mass spectrometer (resolution of ~400; sensitivity of 4×10^{-14} mol/V) with a Balzers SEV 217 electron multiplier using 9–10 cycles of peak-hopping. Data acquisition was performed with the Argus program written by M. O. McWilliams, running under a LabView environment. Blanks were monitored every 3–4 steps and typical ^{40}Ar blanks range from 1×10^{-16} to 2×10^{-16} mol. Ar isotope data corrected for blank, mass discrimination, and radioactive decay are given in Annex S1. Individual errors in Annex S1 are given at the 1σ level.

Details on Diffusion Experiments

The five aliquots (WA-1, WA-2, Chin-3, Thai-3, and Viet-3) were step-heated from 500 °C to 1450 °C. Each extraction step started by 1 min of ramp-up time to take the temperature to the desired value. The temperature was held at the desired temperature for 540 s and was followed by a short temperature drop-off time (approximately 20 s) to a temperature about 200 °C below the degassing temperature, to avoid subsequent gas loss. The temperature was monitored using a thermocouple in direct contact with the crucible containing the samples with a build-in precision equal or better than ±5 °C. We use the K-derived fraction of ^{39}Ar as diffusant and D_0 (the pre-exponential diffusion factor; a theoretical quantity that relates to the average diffusion speed of Ar atoms in the glass at infinite temperature) and E_a (activation energy) were calculated using an Arrhenius plot regression using a spherical geometry with a radius of 175 μm as an average radius size for the glass particles (radius ranging from 150 to 200 μm) and using the equations of Crank and Gupta (1975). The true geometry of each of the glass particles is in fact random as it is the direct result of crushing a glass sphere, and we therefore used a spherical geometry that, in average, best characterize these glass particles that were handpicked. We note that the choice of the geometry has limited impact on the results (Huber et al. 2011). Uncertainties for D_0 and E_a were calculated using the Isoplot linear regression model of –ln (D) versus $10000/T$ and correspond to the scatter of the selected data points around the calculated line (see Fig. 5).

ARGUS VI

Another three aliquots (~120 mg each) from the same three tektites from Thailand (Thai-1), China (Chin-1), and Vietnam (Viet-1) were step-heated using a continuous 100 W PhotonMachine© CO_2 (IR, 10.4 μm) laser fired and rastered on the glass for 60 s. Each of the standard crystals was fused in a single step. The gas was purified in an extra-low-volume stainless steel extraction line of 240 cm^3, using two SAES AP10 and one GP50 getter and cryocooler condensation trap. Ar isotopes were measured in static mode using a low volume (600 cm^3) ARGUS VI mass spectrometer from Thermofisher©, set with a permanent resolution of ~200. Measurements were carried out in multicollection mode using four Faraday cups to measure mass 40 to 37 and a low background compact discrete dynode ion counter to measure mass 36. We measured the relative abundance of each mass simultaneously using 10 cycles of peak-hopping and 16 s of integration time for each mass. Detectors were calibrated to each other electronically and using air shot beam signals.

Analyses at the Laboratoire des Sciences du Climat et de l'Environnement

Tektite fragments from the Chinese (aliquot Chin-2), Thai (Thai-2), and Vietnam (Viet-2) tektites were prepared and analyzed at the Laboratoire des Sciences du Climat et de l'Environnement in France. No Western Australian tektites were analyzed. After crushing and sieving the three samples, tektite glass shards without visible inclusions ranging from 350 μm to up to 1 mm in size were individually handpicked under a binocular (×40 magnification). A total of 100 mg of shards (separates) were finally selected for each tektite and each of the separates was loaded in a single pit hosted in an aluminum disk. Crystals of ACs-2 flux standards were also loaded in the same pit. Samples were irradiated for 60 min (IRR 57) in the β1 tube of the OSIRIS reactor (French Atomic Energy Commission, Saclay, France). After irradiation, for each of the separates, three aliquots (Chin-2, Thai-2, and Viet-2; Table 1) of 50 mg of shards were transferred into a copper sample holder and loaded into a vacuum Cleartran© window. The 50 mg were step-heated using a defocused Synrad CO_2 laser from 4% to 15% of

nominal power (approximately 25 W). Before starting the step-heating process, we slightly degassed each aliquot at 2% of the nominal power. For each step, the Ar isotopes were counted using a VG5400 mass spectrometer equipped with a single ion counter (Balzers© SEV 217 SEN), following the procedures outlined in Nomade et al. (2010). As mentioned above, neutron fluence (J) was monitored by co-irradiation of Alder Creek sanidines standard (ACs-2) (Nomade et al. 2005). J value for each sample was determined from the analyses of two ACs-2 single crystal from each sample. J values were calculated using ACs-2 at 1.1891 ± 0.0006 Ma (Niespolo et al. 2017), the total decay constant of Renne et al. (2011), and the $^{40}Ar/^{36}Ar$ atmospheric ratio of 298.56 ± 0.31 (Lee et al. 2006). Procedural blanks were measured every two or four unknowns. For a typical 10-min static blank, the backgrounds varied from 1.3–4.6 × 10^{-17} to 2.8–6.4 × 10^{-19} mol for ^{40}Ar and ^{36}Ar, respectively. The precision and accuracy of the mass discrimination correction were monitored by weekly measurements of various beam sizes of atmospheric air (see full experimental description in Nomade et al. 2010).

RESULTS

We obtained three plateau ages ranging from 785.0 ± 4.4 ka to 792.1 ± 6.0 ka for the Chinese Vietnamese and Thai tektites measured with the ARGUS VI instrument (Chin-1, Viet-1, and Thai-1; Table 1), two plateau ages of 795 ± 15 ka and 797 ± 15 ka for the Australian tektite measured with the MAP 215-50 instruments (WA-1 and WA-2) (Fig. 3), and three plateau ages ranging from 784 ± 15 ka to 790 ± 19 ka for the Chinese Vietnamese and Thai tektites measured with the VG5400 instrument (Chin-2; Viet-2 and Thai-2; Table 1; Fig. 4). All plateaus include more than 78% ^{39}Ar released and have P-values ≥0.14 (Table 1). Inverse isochron ages are indistinguishable from the plateau ages and range from 784.2 ± 5.5 ka to 795 ± 6 ka (ARGUS VI), 806 ± 24 ka and 792 ± 19 ka (MAP 215-50), and 791 ± 30 ka to 810 ± 55 ka (VG5400) and are shown in supporting information Annex S2 with all results summarized in Table 1. All samples show trapped $^{40}Ar/^{36}Ar$ ratios within the error of the atmospheric composition with values ranging from 295 ± 7 to 299.4 ± 3.3 for the data obtained on the ARGUS VI, 288 ± 20 and 304 ± 16 for the data obtained on the MAP 215-50, and 264 ± 92–302 ± 160 for the data obtained on the VG5400 (Annex S2). All samples show similar average K/Ca ratios (derived from the $^{39}Ar_k/^{37}Ar_{Ca}$ ratios) with values ranging from 0.7 to 1.4 (Annex 1).

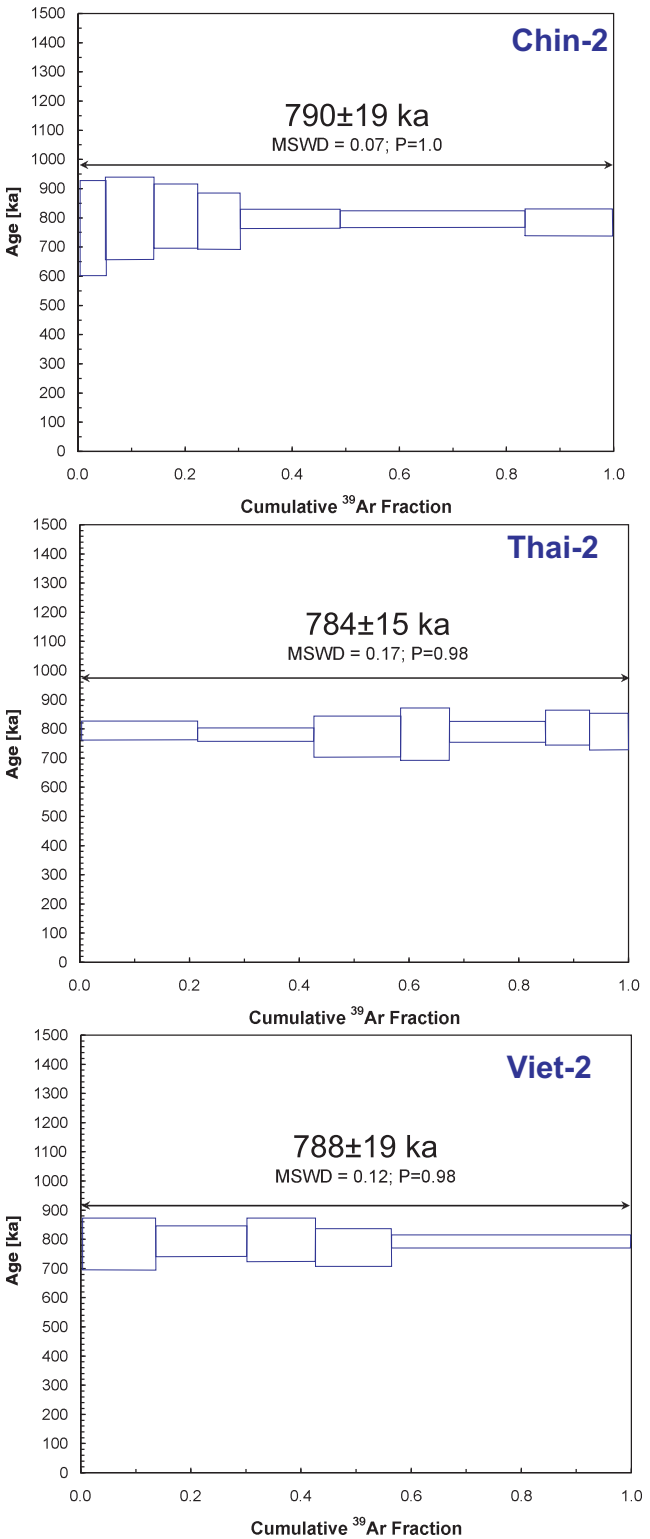

Fig. 4. $^{40}Ar/^{39}Ar$ apparent age obtained at the LSCE laboratory (Gif) with a VG5400 single-collector (blue spectra) instrument for three tektites (Chinese, Thai, and Vietnamese samples). Plateau ages are quoted with 2σ level. (Color figure can be viewed at wileyonlinelibrary.com.)

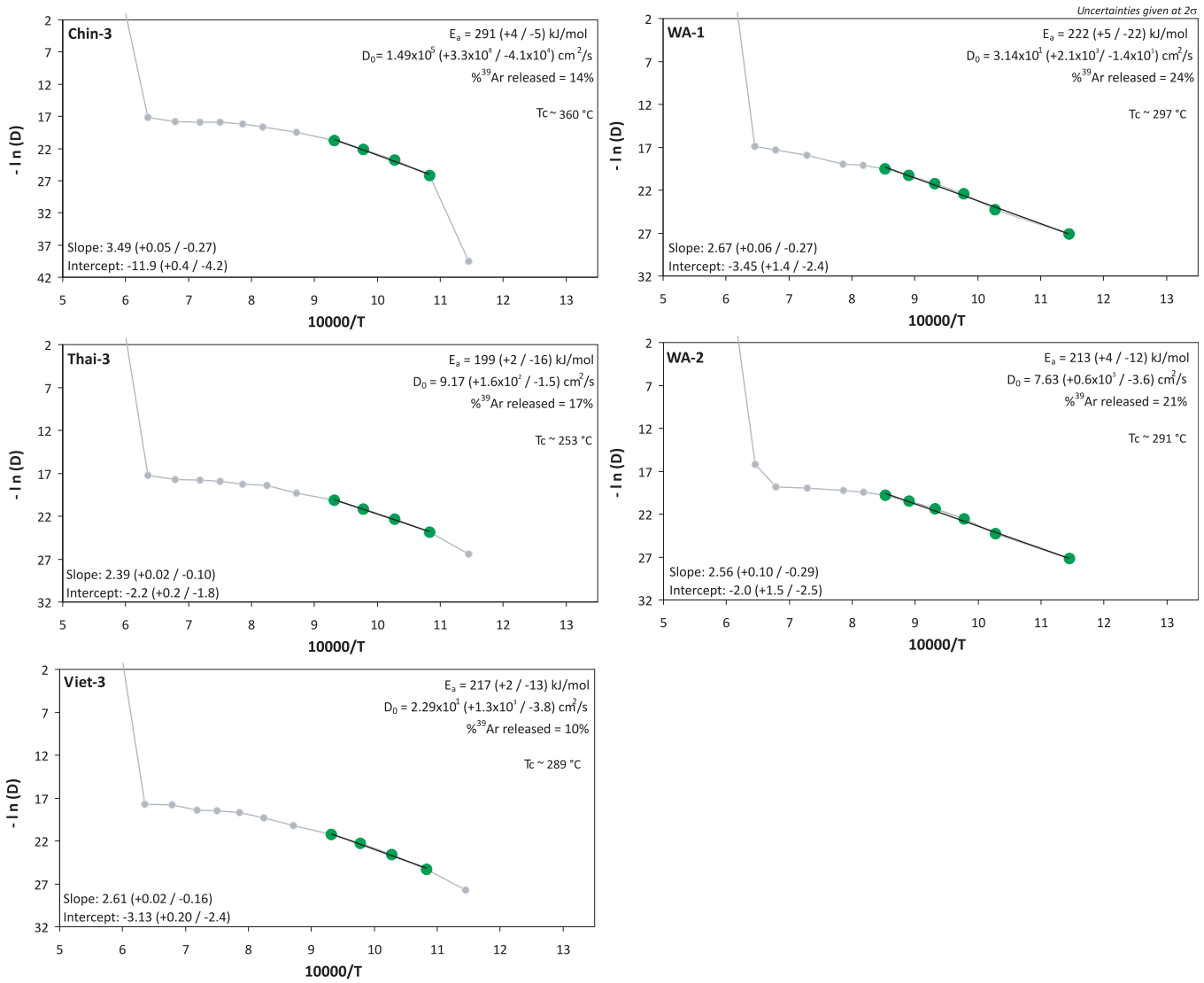

Fig. 5. Arrhenius plot (-ln D versus 10000/T) for five tektites measured using a furnace and a MAP 215-50 mass spectrometer at Curtin University. Slope and intercept values calculated using ISOPLOT are used to determine E_a and D_0 values. All uncertainties indicated at the 1σ level. Data points used in the calculation are indicated by green-filled symbols. (Color figure can be viewed at wileyonlinelibrary.com.)

Diffusion experiments on five aliquots (Chin-3, Thai-3, Viet-3, WA-1, and WA-2) from the four tektites yielded a range of diffusion parameters. The Australian, Vietnamese, and Thai tektites yielded D_0 values ranging from 7.6 to 31.4 cm^2/s and E_a values ranging from 199 to 222 kJ/mol (Table 1; Fig. 5). E_a and D_0 regression uncertainties are provided in Table 1. For reference, these values correspond to closure temperatures of 253–297 °C for a sphere with a 175-μm radius cooling at 10 °C/Ma. The Chinese tektite yielded substantially different values with $D_0 = 1.5 \times 10^5$ cm^2/s and $E_a = 291$ kJ/mol, corresponding to a closure temperature of 360 °C (Fig. 5). Note that the closure temperature concept is a counterintuitive quantity due to the very short time span spent at ultrahigh peak temperatures, and thus, in the present case, the diffusivity speed (D_0) has a much greater positively correlated influence on $^{40}Ar^*$ loss.

DISCUSSION

Age of the Australasian Tektites

All tektites yielded plateau ages and inverse isochrons with $^{40}Ar/^{36}Ar$ intercepts in the error of the atmospheric ratios, suggesting that little to no undesirable effects such as $^{40}Ar^*$ loss or the presence of inherited $^{40}Ar^*$ or alteration products are present. All samples yielded concordant $^{40}Ar/^{39}Ar$ age spectra, and

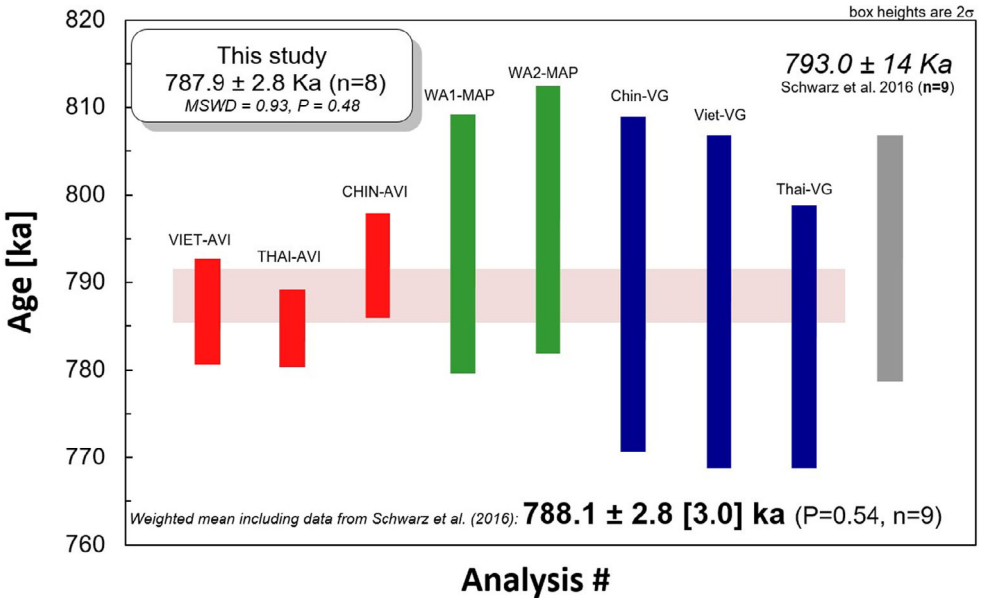

Fig. 6. Summary plot of all the $^{40}Ar/^{39}Ar$ plateau age results obtained in this study using an ARGUS VI (AVI, red), a MAP-215 (MAP, green), a VG5400 (VG, blue). Weighted mean age calculated for all data obtained in this study shown as a horizontal pink box. The weighted mean age (gray) of Schwarz et al. (2016) is shown for comparison. Grand weighted mean including the data from Schwarz et al. (2016) results in an age of 788.1 ± 2.8 Ma [3.0]. The uncertainty in square brackets includes all sources of errors. (Color figure can be viewed at wileyonlinelibrary.com.)

we calculated a mean age (Fig. 6) of 787.9 ± 2.8 [3.0] ka (MSWD = 0.97, P = 0.48) using all the eight plateau ages weighted by the inverse variances of their individual analytical uncertainties. A P-value of 0.48 confirms that this is a single age population and thus, that the tektites were formed during a single event. The uncertainty of [±3.0] includes all sources of errors and was calculated following Renne et al. (2010), using an error propagation approach based on Monte Carlo simulations. We prefer to derive our weighted mean age calculated using the plateau ages rather than the inverse isochron age (789.0 ± 3.4 ka; Table 1) because (1) the inverse isochrons show that all tektites have trapped Ar with an atmospheric composition, and (2) more importantly, the statistical agreement between the plateau ages is much better than the inverse isochron ages (P = 0.48 versus P = 0.06) suggesting that the former age is more robust. The weighted mean age of 788 ± 3 ka is based on nine individual plateau ages measured on three different mass spectrometers equipped with different gas extraction systems and from two different user groups demonstrating that it is not laboratory dependant.

Furthermore, our age is in excellent agreement with the recent age of 793 ± 14 ka proposed by Schwarz et al. (2016) for the Australasian tektites (Figs. 2 and 6). Incorporating the final age recommended by Schwarz et al. (2016), which was calculated using the same set of decay constants, yields an almost identical age of 788.1 ± 2.8 [3.0] ka with a slightly improved probability of fit (P = 0.54). Adding the data from Schwarz et al. (2016) means that our weighted mean age is concordant with data obtained using four mass spectrometers across three laboratories, thus demonstrating the reproducibility and full intercalibration of this age.

Therefore, we propose that the age of 788.1 ± 2.8 [3.0] ka currently represents the best measured age estimate for the formation of the Australasian tektites (Fig. 6). Furthermore, it is important to stress that this age is in excellent agreement with two $^{40}Ar/^{39}Ar$ ages of 792.4 ± 1.0 ka and 785.6 ± 1.4 ka obtained on volcanic ejecta from the Toba volcano that unambiguously bracket the formation of Australasian microtektites (Mark et al. 2017). Based on the latter two $^{40}Ar/^{39}Ar$ ages and a Bayesian age-depth model, those authors proposed that the formation age of the tektite is around 786 ± 4 ka, in perfect agreement with our $^{40}Ar/^{39}Ar$ age of 788 ± 3 ka. Furthermore, the climatostratigraphic position of the Australasian tektites layer in oceanic sediments (first part of termination IX, e.g., Valet et al. 2014) makes this widespread event a major independent tie-point for improving the chronological framework and synchronized paleoclimatic records in the region where the tektites layer is found. It is worth noticing that our high-precision age agrees well with the Australasian tektites age of 790 ± 5 ka estimated by Valet et al. (2014) using astrochronological approach in the MD90-961 (Indian Ocean).

Power of Multicollector Noble Gas Instruments to Date Young Impact Craters

Our new age of 788.1 ± 2.8 ka is about five times more precise than the $^{40}Ar/^{39}Ar$ age of 793 ± 14 ka previously proposed by Schwarz et al. (2016) (Fig. 6). The main reason for the drastic improvement in precision for such a low number of analyses is because some of the data were generated using the ARGUS VI multicollector noble gas mass spectrometer. This instrument generated plateau ages with precision ranging from ±4.4 to ±6 ka compared to ±15 to ±19 ka obtained on the single-collector instruments (MAP 215-50 and VG5400) (Figs. 3, 4, and 6). The three- to fourfold improvement in precision of individual plateau ages is due in part to improved electronic stability of the Faraday cups, but mostly due to the ability to precisely measure the small ^{36}Ar mass on a CDD (ultralow-noise ion counter), which can yield ultraprecise measurements even for extremely small ion beam signals (e.g., Jourdan et al. 2017). Precise measurement of ^{36}Ar is important to correct for trapped (nonradiogenic) ^{40}Ar contribution in a sample, especially for young samples where the amount of $^{40}Ar^*$ produced is still low, and thus, the large mass of sample needed for a precise analysis results in the addition of a substantial amount of naturally trapped argon released during step-heating extraction (Annex 2). The relative precision of ±4‰ (2σ) obtained for the Australasian tektites compares well with the recent improved precision of ±1.4‰ (weighted mean age of 14.808 ± 0.021 Ma) obtained on three glass ejecta from the Ries impact crater (Schmieder et al. 2018), also measured on the ARGUS VI at Curtin University.

This significant improvement in precision is important to assess the simultaneity of impact events with other events such as biotic crises (Renne et al. 2013) and to test simultaneity of impact events (Schmieder et al. 2014). It is equally important when impact ejecta are used similar to volcanic ejecta as stratigraphic markers (Yamei et al. 2000; Mark et al. 2017) and where precision is critical for estimating climate evolution rates (Mark et al. 2017).

Diffusion Loss during Impact—A Window to the *T–t* Condition of the Melt

Relevance of Diffusion Modeling

The most important thing to consider as far as dating a melt particle by $^{40}Ar/^{39}Ar$ is concerned is the ability for the melt to be purged of all its inherited $^{40}Ar^*$, which is accumulated in the rock prior to the impact; that is, that the K/Ar clock is fully reset at the time of the impact (Jourdan et al. 2007). This is related to the efficiency (i.e., speed) at which the melt is able to release the $^{40}Ar^*$, hence is related most directly to the D_0 value (the higher the value, the faster $^{40}Ar^*$ can leave the melt) and the time spent close to the peak temperature where the melt can most efficiently get rid of its inherited $^{40}Ar^*$. This, in turn, can be reverted to estimate the *T–t* history of a given melt particle, and thus provide semiquantitative constraints about the conditions at the time of impact.

Tektites are an ideal candidate to test those conditions because their current size is known and some of them have roughly spherical shapes with relatively short heating and subsequent cooling durations, contrary to melt rocks for which these quantities are not known. Nowak et al. (2004) experimentally determined the diffusion parameters (i.e., D_0 and E_a) of argon in silicate melts. Based on these parameters, Jourdan et al. (2007) modeled the effect of inherited $^{40}Ar^*$ loss during impact as a function of the melt composition, showing that mafic melts will have significantly more chance to be fully degassed whereas silicic melts being substantially more polymerized and viscous will likely contain significant amount of inherited $^{40}Ar^*$.

The D_0 and E_a pair diffusion values measured on four tektites range from 7.6 to 1.5×10^5 cm^2/s and 199 to 291 kJ/mol (Table 1; Fig. 5). The variation in those values most likely corresponds to a variation in composition of the melt (Nowak et al. 2004; Jourdan et al. 2007). These values can be compared with diffusion experiments by Nowak et al. (2004) at 500 MPa on iron-free mafic (D_0 ~45 cm^2/s; E_a ~257 kJ/mol; closure temperature ~380 °C) and silicic synthetic melts (D_0 ~5.9×10^{-2} cm^2/s; E_a ~182 kJ/mol; closure temperature ~266 °C), and more recently from Amalberti et al. (2018) on an iron-free synthetic mafic melt at 0.1 MPa (D_0 ~1.7×10^{-2} cm^2/s; E_a ~137 kJ/mol; closure temperature ~150 °C). Compared to our results on tektite glass, this suggests that there is no significant difference between the diffusivity characteristics of a melt and its glass counterpart. One important thing to note is that the presence of primary water in the melt significantly enhanced the argon degassing efficiency of melt particles (Zhang et al. 2007; Mark et al. 2014) but is hard to quantify in the case of tektites because the water left the system during melt stage.

The geochemical composition of the tektites analyzed in this study is not known, although Schwarz et al. (2016) compiled available major and trace element analyses for the Australasian tektites. The composition of all the Australasian tektites ranges from approximately 62–82 wt% SiO_2 and 3–5 wt% $Na_2O + K_2O$ (Chapman and Scheiber 1969), implying that they quenched from a substantially evolved melt which would correspond to tholeiitic lavas with dacitic

Table 2. Summary table of argon diffusion data for 5 of the 11 aliquots from four different tektites, showing diffusion characteristics.

	General characteristics				Diffusion characteristics						
Sample	Initial diameter (cm)	Aliquot #	Instrument used	Extraction system	D_0 (cm^2/s; 1σ)	+	−	E_a (kJ/mol;1σ)	+	−	Amount of ^{39}Ar (%)
Chin	~1.5 cm	Chin-1	ARGUS VI	Laser				N/A[a]			
		Chin-2	VG5400	Laser				N/A[a]			
		Chin-3	MAP215-50	Furnace	1.49E+05	3.8E+08	4.1E+04	291	4	5	14%
Thai	~1 cm	Thai-1	ARGUS VI	Laser				N/A[a]			
		Thai-2	VG5400	Laser				N/A[a]			
		Thai-3	MAP215-50	Furnace	9.17	1.6E+02	1.5E+00	199	2	16	17%
Viet	~0.8 cm	Viet-1	ARGUS VI	Laser				N/A[a]			
		Viet-2	VG5400	Laser				N/A[a]			
		Viet-3	MAP215-50	Furnace	2.29E+01	1.3E+03	3.8E+00	217	2	13	10%
WA	~1.5 cm	WA-1	MAP 215-50	Furnace	3.14E+01	2.1E+03	1.4E+01	222	4	5	24%
		WA-2	MAP 215-50	Furnace	7.63	6.0E+02	3.6E+00	213	4	12	21%

[a]Not available as measured with a laser without temperature control.

to rhyolitic compositions. However, the diffusion characteristics of the tektites analyzed in this study make them more prone to quick diffusion than the rhyolitic melt measured by Nowak et al. (2004). In practice, (1) the composition of the rhyolitic melt from Nowak et al. (2004) is synthetic and alkaline (~8 wt% of $Na_2O + K_2O$), and (2) has a lower amount of CaO (~1.3 wt% versus an average of ~2.4 wt% for the Australasian tektites), the presence of which has been shown to decrease viscosity and increase thermal diffusivity (Hofmeister et al. 2014).

To test which *T–t* conditions are required for the various tektites to lose all their inherited $^{40}Ar^*$, we performed argon diffusion models based on the characteristics (D_0, E_a, original size) measured for the tektites. Following Jourdan and Eroglu (2017), we used two different approaches to simulate the effect of inherited $^{40}Ar^*$ loss of a sphere with a diameter of 1 cm (or 1.5 cm in the case of the Chinese tektites, cf. below) and with an arbitrary initial age of 1.5 Ma assumed to represent the age of the target rock (none of the conclusions are affected by the choice of this age). (1) We use the ArArDIFF algorithm (Jourdan and Eroglu 2017; Jourdan et al. 2017), which allows the modeling of ^{40}Ar transport in a sphere by diffusion and thus, calculating the effect of given *T–t* histories on the shape of a synthetic age spectrum and (2) we use a forward modeling Monte Carlo approach applied to a simplified sets of diffusion equations from McDougall and Harrison (1999) for a sphere. This approach can accommodate a large number of adjustable parameters and partially take into account the uncertainties of D_0 and E_a measured in this study. Details of each model and their results are provided below and in Table 2.

Modeling of Synthetic Age Spectra

We used the diffusion values of the Chinese tektite (high diffusivity) and the Thai tektite where we use the average measured D_0 and E_a values (7.6 cm^2/s and 199 kJ/mol; low diffusivity) and the most diffusive values within the uncertainties (1σ) of the measurements from the Thai tektite (Fig. 5; D_0 = 178 cm^2/s; E_a = 201 kJ/mol; average diffusivity). Cavosie et al. (2018) recently estimated a *minimum* temperature of the melt of ~1700 °C based on the presence of reidite reverted to zircon in the glass of Muong Nong Thai tektites that we used as the starting temperature for our models. Stöffler et al. (2002) carried out hydrocode-based numerical simulations of cm-sized tektites to understand the *T–t* path and formation regimes of moldavites. In some scenarios, their model suggests that for some tektites, the peak temperature will be ~3100 °C gradually decreasing down to 1100 °C for 10 s followed by a decrease in temperature from 1100 to 700 °C for the following 20 s. Those relatively long cooling durations are due to the fact that the tektite travelled (at least partially) in an entraining gaseous medium, at a predicted temperature of 700–1700 °C, allowing the particles to stay molten for an extended time (Stöffler et al. 2002). We also use this cooling phase duration as a starting point of our models. To those conditions, we added a postcooling time of 10 min to 25 °C. However, we note that neither of the two cooling periods below 1100 °C have any influence on $^{40}Ar^*$ loss due to the short durations involved.

Our model shows that a peak temperature of 1700 °C and subsequent cooling to 1100 °C with a duration of 10 s is largely insufficient to reset the K/Ar clock and release all the inherited $^{40}Ar^*$ in the Thai

Table 3. Parameters used in the various Monte Carlo diffusion models presented in this study. Range of values, approximate function distribution, and distribution parameters are indicated.

Simulated parameter	Range of values	Distribution	Distribution curve parameters
General simulations (Fig. 8)			
Peak temperature	1700–6371 °C[a]	Weibull	Offset = 1700 °C; Shape = 1; Scale = 1000 °C
Radius	500–20,000 microns[a]	Triangular	Mode = 500 microns
Duration of cooling time from peak temperature to 1100 °C	5–30 s	Uniform[b]	N/A
E_a	199–456 kJ/mol[a]	Gamma	Offset = 199 kJ; Shape = 1; Scale = 30 kJ
D_0[c]	1.7–1.7 × 10^6 cm²/s[a]	N/A	
Thai tektite simulations (Figs. 10a & 10c)—Fixed D_0 and E_a			
Peak temperature	1700–6371 °C[a]	Weibull	Offset = 1700 °C; Shape = 1; Scale = 1000 °C
Duration of cooling time from peak temperature to 1100 °C	5–30 s	Uniform	N/A
Thai tektite simulations (Figs. 10b and 10d)— D_0 and E_a with uncertainties			
Peak temperature	1700–6371 °C[a]	Weibull	Offset = 1700 °C; Shape = 1; Scale = 1000 °C
Duration of cooling time from peak temperature to 1100 °C	5–30 s	Uniform[a]	N/A
E_a	191–201 kJ/mol	Gamma	Offset = 199 kJ; Shape = 1; Scale = 30 kJ
D_0	7–172 cm²/s	Triangular	Mode = 9.7 cm^2/mol

[a]This range included 99% of the simulations. The function favors the low range of values.
[b]Homogenous: every value within this range has the same probability.
[c]Not a direct input. Calculated using the function: y = 4E-10xe0.0001 E_a (R2 = 0.97).

tektite, and even the diffusive Chinese tektite with as much as 95% of inherited ^{40}Ar* left in the system after cooling (Fig. 7a). Increasing the cooling duration to 30 s yields very similar results (Fig. 7b) for both tektites. Increasing the peak temperatures to 2900 °C and 2450 °C for durations of 10 and 30 s, respectively, will allow full reset of the high diffusivity Thai tektite, but not of the Thai tektite with average diffusivity (Figs. 7c and 7d). Finally, temperatures of 4800 °C (10 s) and 3950 °C (30 s) will reset the Thai tektite with an average diffusivity (Figs. 7e and 7f).

Taking into account uncertainties in the diffusion parameters, our models suggest that the Thai tektite from this study immediately upon impact reached a minimum peak temperature between 2450 °C and 3950 °C (Figs. 7d and 7f) followed by cooling over several tens of seconds to the solidus temperature.

Monte Carlo Simulation Models—Large Number of Variables

Because the number of adjustable parameters for generic tektites is relatively large compared to the model above, and with each parameter having a range of possible values and quantities such as E_a and D_0 having associated uncertainties (Fig. 5), we employed a forward modeling approach using Monte Carlo simulations to test the effect of a large range of values on the total inherited ^{40}Ar* loss that can be experienced by a wide variety of tektites with various diffusion parameters.

We simulated 10,000 trials using the statistical software package Quantum XL©, a commercially available Excel add-on from Sigmazone© while varying the following parameters within realistic ranges (Table 3): (1) the total duration of the drop from peak temperature to 1100 °C (approximating the solidus temperature) with a possible duration from 5 to 30 s following a uniform distribution between those two values; (2) the radius of the tektite varying from 500 μm to 2 cm with a triangular distribution and with a mode defined at 500 μm which approximates the larger abundance of small tektites compared to large ones; (3) the E_a energy using a Gamma distribution with an offset (mode) at 199 kJ/mol, a shape of 1, and a scale of 30 kJ (approximating the larger abundance of tektite with low diffusivity as observed in our data set); and (4) the peak temperature using a Weibull function and an offset (mode) of 1700 °C a shape of 1 and a scale of 1000 °C favoring the low range of temperatures. Note that the E_a and D_0 values tend to be positively correlated, so D_0 was not considered as an input in our simulation, but was rather calculated following an exponential function (Table 3; R^2 = 0.97). Finally, note that all functions and their offset have been selected to favor the low temperature range (i.e.,

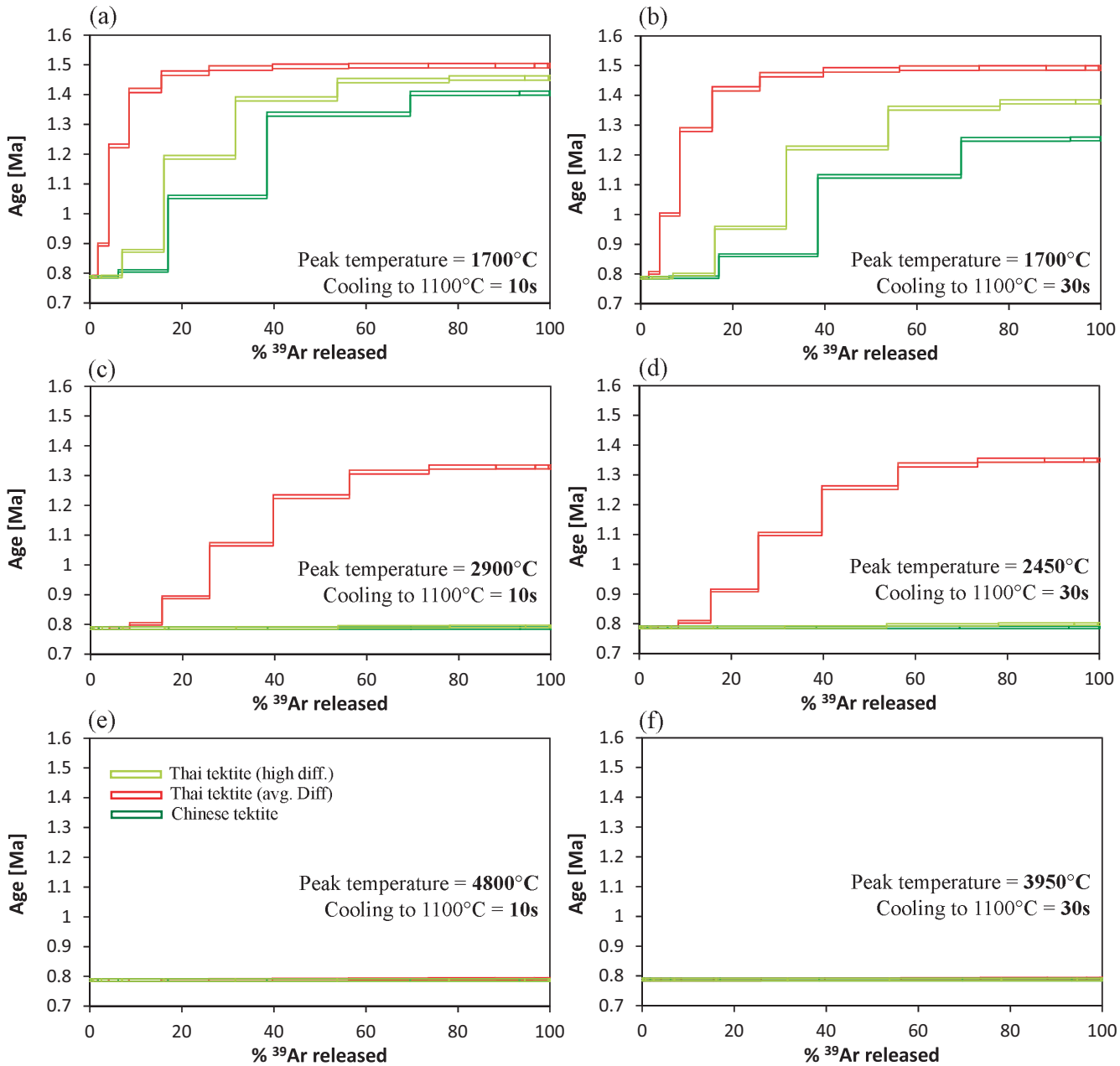

Fig. 7. Modeled age spectra for a 5-mm radius sphere with a pre-$^{40}Ar^*$ loss age of 1.5 Ma calculated using the ArArDIFF algorithm (Jourdan and Eroglu 2017; Jourdan et al. 2017). We simulate various peak temperature values followed by a cooling phase down to 1100 °C (~solidus temperature) of either 10 s or 30 s, and subsequent cooling phases from 1100 °C to 700 °C for the following 20 s and from 700 °C to 25 °C for the following 10 min. Note that neither of the two cooling phases below 1100 °C has any noticeable influence on the total $^{40}Ar^*$ loss due to the short durations involved. Light green spectra (Thai tektite with high diffusivity; D_0 = 178 cm^2/s; E_a = 201 kJ/mol), red spectra (Thai tektite with average diffusivity; D_0 = 7.6 cm^2/s; E_a = 199 kJ/mol), and dark green spectra (Chinese tektite with very high diffusivity; $D_0 = 1.5 \times 10^5$ cm^2/s; E_a = 291 kJ/mol). Diffusion parameters and uncertainties given in Table 1 and Fig. 5. (Color figure can be viewed at wileyonlinelibrary.com.)

more simulation points at low temperatures compared to high temperatures) since we are interested in quantities such as the minimum possible temperature where full $^{40}Ar^*$ diffusive loss occurs.

Figure 8 illustrates the results of the Monte Carlo simulations and shows the amount of $^{40}Ar^*$ loss versus peak temperature (Fig. 8a) and tektite radius (Fig. 8b). As expected with Monte Carlo simulations involving

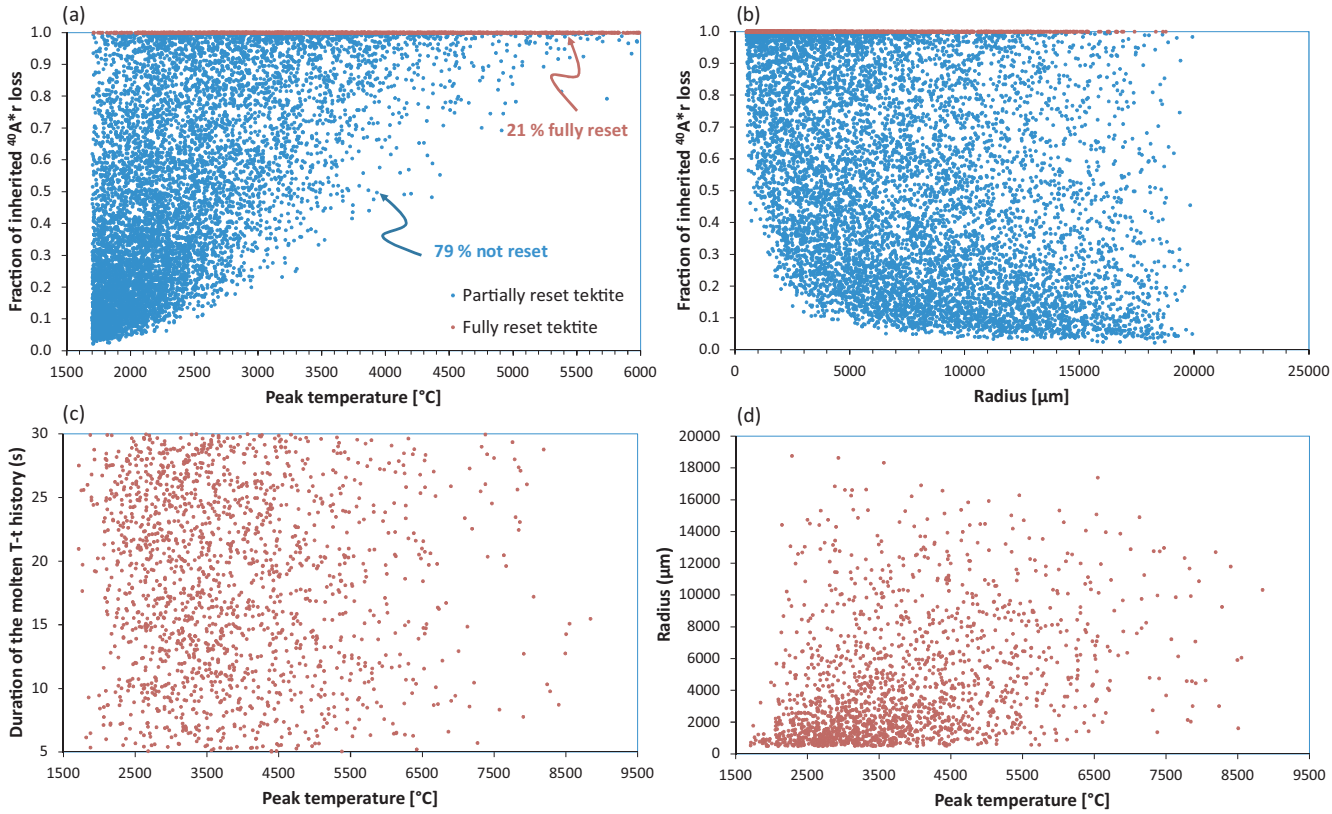

Fig. 8. Monte Carlo simulations (10,000 trials per simulation) of the ^{40}Ar* loss of glass spheres with variable characteristics and variable time–temperature histories following impact. Parameters of the simulations are given in Table 1 and in the text. Results with partial ^{40}Ar* loss are indicated in blue; results with total ^{40}Ar* loss (< 0.01% ^{40}Ar* left) are indicated in red. a) Peak temperature versus ^{40}Ar* loss, (b) radius versus ^{40}Ar* loss, (c) duration of the cooling phase between peak temperature and 1100 °C, and (d) peak temperature versus radius. (Color figure can be viewed at wileyonlinelibrary.com.)

many variables (e.g., Jourdan and Eroglu 2017), the plots show a large range of results making it impossible on a two-dimensional plot to find cutoff values at which total ^{40}Ar* loss occurs. The graph in Fig. 8a shows that complete resetting can be achieved at temperatures as low as 1700 °C (probably due to a combination of very small radius and high D_0) but in other cases will not be achieved at temperatures up to 4500 °C (probably for the largest and most viscous tektites). The graph also shows empty zones which correspond to impossible scenarios; for example, above 4500 °C, it is expected that every tektite should have at least 55% ^{40}Ar* loss regardless of its size or diffusion characteristics. Figure 8b shows a less well-defined covariation but indicates similarly that tektites smaller than 1 mm radius should undergo at least 45% ^{40}Ar* loss regardless of their T–t history.

Plotting a "tornado chart" (Fig. 9), which illustrates the relative importance of factors contributing most significantly to the variation in ^{40}Ar* loss (Jourdan and Eroglu 2017), shows that the most important factor is the peak temperature immediately after impact, which is responsible for 60% of the argon loss variation (the higher the temperature, the higher the ^{40}Ar* loss). The second most important factor is the size of the tektites, which is responsible for 28% of all variation. This means that within the range of parameters used in the model, approximately 90% of argon loss is controlled by the peak temperature and tektite size. Perhaps more surprisingly, only 21% of all simulations show the complete resetting of inherited ^{40}Ar* (defined as 0.1% or less ^{40}Ar* remaining in the system). If the range of parameters we used is correct, this suggests that only one in five tektites analyzed by ^{40}Ar/^{39}Ar should yield a flat plateau (but see discussion below).

Monte Carlo Simulation Models—Restricted Number of Variables

In the case of the tektites analyzed in this study, some of the parameters are known and we can use a similar Monte Carlo simulation approach to interrogate the possible T–t history of a particular tektite further without including a very large range of possible scenarios.

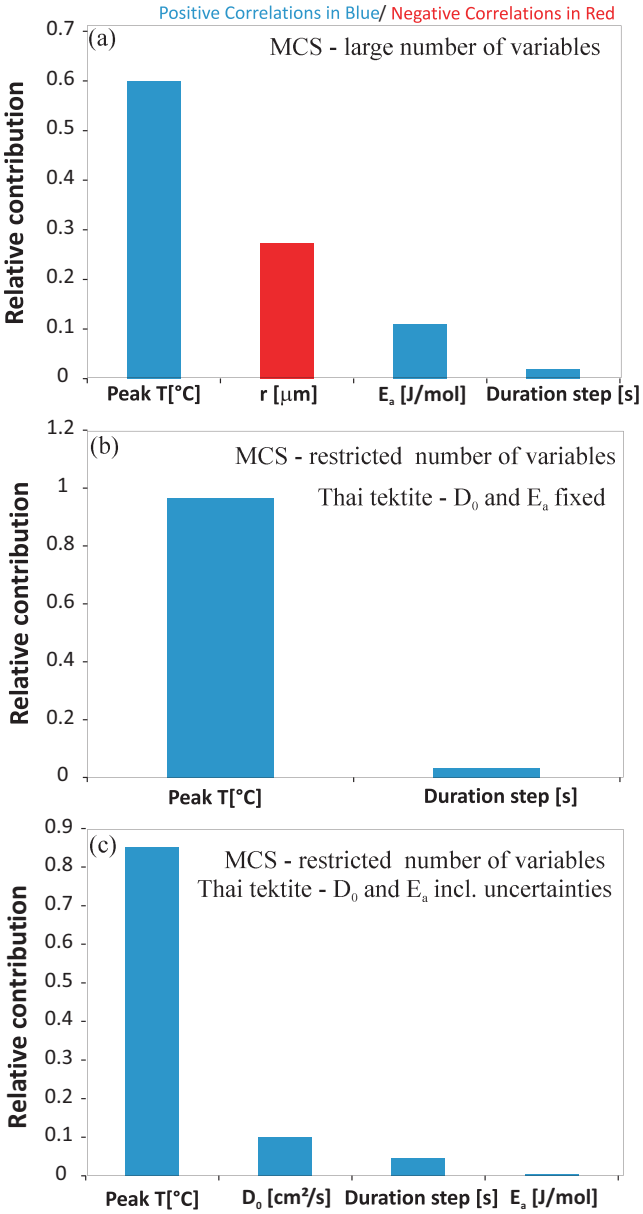

Fig. 9. Tornado chart showing the relative weight of the factors contributing to the inherited $^{40}Ar^*$ loss (e.g., the most influential factor in all simulations is systematically the peak temperature). All the boxes sum to 1. Chart for the general Monte Carlo simulations shown in Fig. 8 (a), Figs. 10a and 10c (b; fixed D_0 and E_a values), and Figs. 10b and 10d (c; D_0 and E_a including uncertainties). Positive correlations with diffusion loss are indicated in blue; negative correlations are indicated in red. (Color figure can be viewed at wileyonlinelibrary.com.)

In the following simulations, we use the radius, E_a, and D_0 values (Table 1) of the Thai tektite to test which scenarios would result in complete $^{40}Ar^*$ loss. In the first set of simulations, we set the D_0 and E_a value to their average values (i.e., 9.2 cm^2/s and 199 kJ). In the second set of simulations, we vary these quantities within 1σ of the uncertainty reported in Fig. 5 for the Thai tektite using a triangular distribution centered around the average value (D_0 varies from 7.6 to 178 cm^2/s and E_a varies from 191 to 201 kJ/mol).

In the case of the strict D_0 and E_a scenario, only 7% of the tested scenarios yielded T–t pairs high enough to fully reset $^{40}Ar^*$ (Fig. 10). There are only two variables, but the contribution factor analysis (Fig. 9b) indicates that in fact, 97% of the variation is controlled by the peak temperature value. In other words, the time it takes for the tektites to cool down from the peak temperature has a negligible role on $^{40}Ar^*$ loss. This model suggests that resetting (less than 0.1% $^{40}Ar^*$ left) of the $^{40}Ar^*$ should not be expected below ~3960 °C (Figs. 10a and 10c). This temperature is in excellent agreement with the synthetic $^{40}Ar/^{39}Ar$ age spectra obtained for the average diffusive Thai tektite using ArArDIFF (~3950 °C; Fig. 7f) considering that somewhat different approaches were used. Complete purging (0% $^{40}Ar^*$ left) requires peak temperatures higher than 4350 °C.

For the second scenario (uncertainties in the D_0 and E_a values included in the model), Figs. 10c and 10d show that the results are significantly different due to the higher possible values for D_0 (up to 172 cm^2/s). About 31% of all simulations resulted in complete $^{40}Ar^*$ loss from the tektites (Fig. 10c). In those models, 85% of the variation was controlled by the peak temperature, and 10% controlled by the D_0 value. This model suggests that resetting (less than 0.1% $^{40}Ar^*$ left) should not be expected below ~2350 °C (Fig. 10d), which is similar to the peak temperature of ~2450 °C derived from ArArDIFF (Fig. 7d). Complete purging (0% $^{40}Ar^*$ left) requires peak temperatures higher than 2550 °C.

Similar simulations using the diffusion parameters of the 1.5-cm diameter Chinese tektite show that 57% of the scenarios interrogated yield complete $^{40}Ar^*$ loss (less than 0.1% $^{40}Ar^*$ left), with 83% of the total variation due to the peak temperature and 17% due to the total duration of the molten state (not shown). More importantly, this model suggests that temperatures as low as 2010 °C are able to reset the Chinese tektite and that any scenarios with peak temperature above 2350 °C will always result in resetting the $^{40}Ar^*$ in the tektite.

Limitations of the Diffusion Models

In practice, $^{40}Ar^*$ diffusion modeling applied to tektites has its own limitations, with various competing factors that all might influence the temperature estimates given above. For example, the presence of primary water in the melt before evaporation is likely to increase diffusivity parameters during the first few seconds (Mark et al. 2014). However, modeling on the effect of water on the diffusion of $^{40}Ar^*$ in glass by Mark et al. (2014) shows that the presence of water greatly affects E_a but

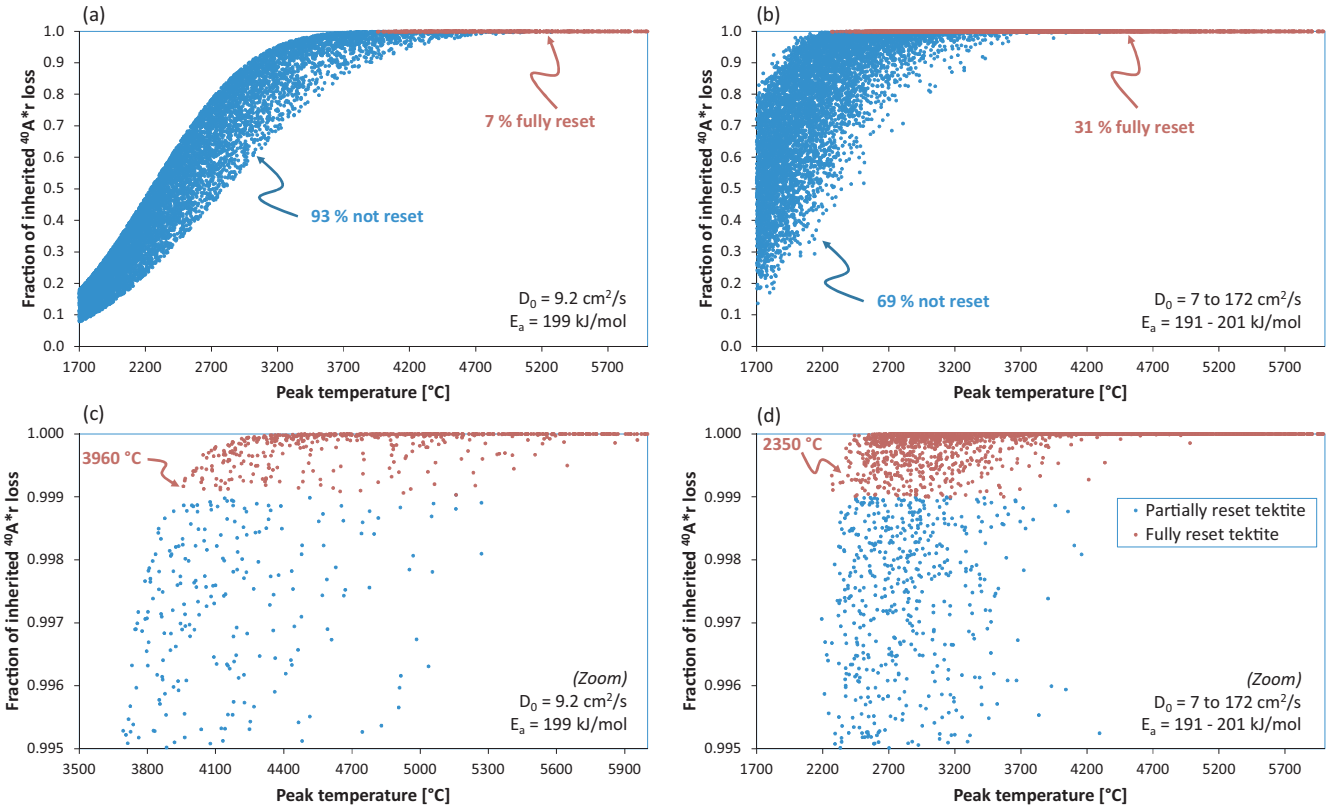

Fig. 10. Monte Carlo simulations (10,000 trials per simulation) of the fraction of ^{40}Ar* loss of tektite spheres using the diffusion parameters of the Thai tektite (Fig. 5) with variable peak temperatures and cooling phase durations. Parameters of the simulations are given in Table 1 and in the text. (a) and (c) simulations using the average measured D_0 and E_a values without uncertainties and (b) and (d) using D_0 and E_a values of the Thai tektite including their uncertainties. Diffusion parameters used in the simulation are provided. (Color figure can be viewed at wileyonlinelibrary.com.)

does not change the D_0 value. Figure 9 shows that E_a contributes to less than 1% of the variance of ^{40}Ar* loss, suggesting that initial water does not influence the ability to calculate peak temperatures for very brief events like tektite formation. Because tektites are viscous bodies in motion in a viscous medium (Moynier et al. 2009), they will probably experience advection during their molten stage, which in turn can speed up ^{40}Ar* loss (causing overestimation of peak temperature values), but the effect of advection is hard to quantify. Conversely, radius reduction due to vaporization at high temperature and travel in a viscous medium might cause underestimation of peak temperature values.

Significance of Diffusion Models and Peak Temperature Estimates

Using a wide range of conditions, our Monte Carlo model applied to generic tektites (Fig. 8) predicts that only 21% of all tektites analyzed should yield a 99.999% reset and thus generate a plateau age. Yet, *none* of the five tektites analyzed in this study show the presence of excess Ar. Literature ^{40}Ar/^{39}Ar data show no inherited ^{40}Ar* (Lo et al. 2002; Lee et al. 2004) to very little inherited ^{40}Ar* (Yamei et al. 2000; Schwarz et al. 2016). In detail, however, the full step-heating data of Schwarz et al. (2016) from one Thailandite and one Javanite show that, despite yielding mini-plateaus (comprising 50–70% of total ^{39}Ar released) with ages within error of the impact age of 788 ± 3 ka, exhibit the clear presence of inherited ^{40}Ar* at high-temperature steps. Furthermore, earlier K/Ar results from McDougall and Lovering (1969) on button flange tektites and recalculated and summarized by Schwarz et al. (2016) show in fact the systematic presence of excess ^{40}Ar* in most samples. Nevertheless, button flange tektites tend to be *several* cm in diameter, and thus harder to reset as suggested by our general Monte Carlo simulations (Fig. 8b). Considering the discrepancy between the amount of inherited ^{40}Ar* predicted and generally observed, and because the most important factor controlling the inherited ^{40}Ar* loss is likely to be the peak temperature (Fig. 9), we interpret such a discrepancy as indicating that the natural peak temperature conditions of tektite formation should

therefore be in the upper range of what we used in our general models.

All but the Chinese tektite analyzed in this study show relatively average diffusivity characteristics. Detailed ArArDIFF modeling (Fig. 7) and Monte Carlo simulations (Figs. 8 and 10) suggest that the minimum peak temperature required to reset the Thai tektite with average diffusivity characteristics is 3950 °C. If uncertainties in our diffusion measurements are taken into account, the absolute minimum peak temperature needed to fully reset the Thai tektite is 2350 °C. We therefore interpret the results of our diffusion models as suggesting that a *minimum* peak temperature value between 2350 and 3950 °C was needed to reset the Thai tektite (as well as the Vietnamese and Australian tektites with similar diffusion characteristics), hence a *strict minimum* value of 2350 °C. A value of ≫2350 °C is compatible with (1) the minimum peak temperatures suggested by the presence of reidite in some Thai tektites (>1700 °C; Cavosie et al. 2018), particularly considering that these tektites had nondigested crystals likely suggesting a lower peak temperature compared to their crystal-free counterparts, (2) the presence of cubic zirconia in the Mistastin impact melt rock (>2400 °C; Timms et al. 2017), (3) the temperature derived from hydrocode-based numerical simulations of the Moldavite genesis (~3100 °C; Stöffler et al. 2002) and hydrocode models of Collins et al. (2012) suggesting postshock temperatures in excess of 4500 °C in the melt rock at the surface of a crater 1 s after impact. Peak temperatures ≫2350 °C are in agreement with the observation that Cu and Zn isotopes are fractionated (Moynier et al. 2009, 2010) although no temperature was provided in these models. It is also in agreement with the elemental fractionation trend observed for the Transantarctic mircotektites (Folco et al. 2010) where independent laser experimental calibrations suggest temperatures between approximately 3000 °C and 5000 °C (Gerasimov et al. 2005). Finally, we note that our minimum temperature also agrees well with some recent chemical diffusion experiments based on the presence of lechatelierite inclusions within tektites suggesting *T–t* history solutions ranging between 2000 °C maintained for 70 s and 2400 °C maintained for 3 s (Macris et al. 2018). As a caveat, we note that temperatures in excess of 2350 °C do not agree well with the lack of fractionation observed for K isotopes, which suggests temperatures ≤2000 °C (Humayun and Koeberl 2004), although the latter value also conflicts with some of the peak temperature values mentioned above.

In the second part of our study, we demonstrated that coupling diffusion parameter measurement and modeling can provide important information on the *T–t* regime of tektite formation. As a follow-up study, analyzing very large inherited $^{40}Ar^*$-bearing or inherited Ar*-free tektites will enable calculation of the maximum peak temperature experienced by tektites up to full evaporation in any of the four strewn fields. Conversely, if only geochronology is of interest, we advise researchers to focus on the smallest possible (mini)-tektites that can be dated with a sufficient enough precision to avoid any inherited $^{40}Ar^*$.

CONCLUSIONS

Our new multilaboratory and multi-instrument $^{40}Ar/^{39}Ar$ age and diffusion analyses on tektites from Vietnam, China, Thailand, and Australia allow us to draw the following conclusions.

We obtained an age of 788.1 ± 2.8 ka (±3.0 ka, including all sources of uncertainties) that constrains the time of formation of the Australasian tektites. This age is in agreement with precisely dated volcanic markers from the Toba volcano which bracket the formation age of the Australasian microtektites. Our new age is four to five times more precise compared to previous results thanks in part to the multicollection capabilities of the ARGUS VI noble gas mass spectrometer.

Temperature-controlled furnace experiments on the Thai, Vietnamese, and Australian tektites yielded D_0 and E_a values ranging from 7.6 to 31.4 cm^2/s and 199–222 kJ/mol, whereas the Chinese tektite yielded substantially different values with a D_0 value of 1.5×10^5 cm^2/s and E_a of 291 kJ/mol.

Synthetic age spectra and Monte Carlo diffusion models suggest that the minimum temperature of the formation of the Thai tektite is between 2350 °C and 3950 °C; hence, a *strict minimum* value of 2350 °C is in agreement with mineralogical and numerical modeling evidence. This approach should be used on a large number of tektites to constraint the time–temperature regime experienced by melt ejecta during impact events.

Acknowledgments—We thank C. Mayers and A. Frew for their help in the WAAIF during sample preparation. The WAAIF laboratory is supported by an AuScope grant. We are in debt for the thorough reviews from an anonymous reviewer and W. Schwarz who both help us to substantially improve the manuscript. MTDW publishes with permission of the Executive Director of the Geological Survey of Western Australia.

Editorial Handling—Dr. Christian Koeberl

REFERENCES

Amalberti J., Burnard P., Tissandier L., and Laporte D. 2018. The diffusion coefficients of noble gases (HeAr) in a

synthetic basaltic liquid: One-dimensional diffusion experiments. *Chemical Geology* 480:35–43.

Baksi A. K., Archibald D., and Farrar E. 1996. Intercalibration of $^{40}Ar^{39}Ar$ dating standards. *Chemical Geology* 129:307–324.

Beran A. and Koeberl C. 1997. Water in tektites and impact glasses by fourier-transformed infrared spectrometry. *Meteoritics & Planetary Science* 32:211–216.

Cavosie A. J., Timms N. E., Erickson T. M., and Koeberl C. 2018. New clues from Earth's most elusive impact crater: Evidence of reidite in Australasian tektites from Thailand. *Geology* 46:203–206.

Chapman D. R. and Scheiber L. C. 1969. Chemical investigation of Australasian tektites. *Journal of Geophysical Research* 74:6737–6776.

Collins G. S., Melosh H. J., and Osinski G. R. 2012. The impact-cratering process. *Elements* 8:25–30.

Cosca M., Stunitz H., Bourgeix A. L., and Lee J. P. 2011. $^{40}Ar^*$ loss in experimentally deformed muscovite and biotite with implications for $^{40}Ar/^{39}Ar$ geochronology of naturally deformed rocks. *Geochimica et Cosmochimica Acta* 75:7759–7778.

Crank J. and Gupta R. S. 1975. Isotherm migration method in 2 dimensions. *International Journal of Heat and Mass Transfer* 18:1101–1107.

Folco L., D'Orazio M., Tiepolo M., Tonarini S., Ottolini L., Perchiazzi N., Rochette P., and Glass B. P. 2009. Transantarctic Mountain microtektites: Geochemical affinity with Australasian microtektites. *Geochimica et Cosmochimica Acta* 73:3694–3722.

Folco L., Glass B. P., D'Orazio M., and Rochette P. 2010. A common volatilization trend in Transantarctic Mountain and Australasian microtektites: Implications for their formation model and parent crater location. *Earth and Planetary Science Letters* 293:135–139.

Gerasimov M., Yakovlev O., Dikov Y. P., and Wlotzka F. 2005. Evaporative differentiation of impact-produced melts: Laser-simulation experiments and comparison with impact glasses from the Logoisk crater. *Special Paper of the Geological Society of America* 384:351–366.

Glass B. P. and Koeberl C. 2006. Australasian microtektites and associated impact ejecta in the South China Sea and the Middle Pleistocene supereruption of Toba. *Meteoritics & Planetary Science* 41:305–326.

Hofmeister A. M., Whittington A. G., Goldsand J., and Criss R. G. 2014. Effects of chemical composition and temperature on transport properties of silica-rich glasses and melts. *American Mineralogist* 99:564–577.

Huber C., Cassata W. S., and Renne P. R. 2011. A lattice Boltzmann model for noble gas diffusion in solids: The importance of domain shape and diffusive anisotropy and implications for thermochronometry. *Geochimica et Cosmochimica Acta* 75:2170–2186.

Humayun M. and Koeberl C. 2004. Potassium isotopic composition of Australasian tektites. *Meteoritics & Planetary Science* 39:1509–1516.

Izett G. and Obrandovich J. 1992. Laser-fusion 40Ar/39 age of Australasian tektites. *23rd Lunar and Planetary Science Conference*. p. 593.

Jourdan F. 2012. The $^{40}Ar/^{39}Ar$ dating technique applied to planetary sciences and terrestrial impacts. *Australian Journal of Earth Sciences* 59:199–224.

Jourdan F. and Eroglu E. 2017. $^{40}Ar/^{39}Ar$ and (U-Th)/He model age signatures of elusive Mercurian and Venusian meteorites. *Meteoritics & Planetary Science* 52:884–905.

Jourdan F. and Renne P. R. 2007. Age calibration of the Fish Canyon sanidine Ar-40/Ar-39 dating standard using primary K-Ar standards. *Geochimica et Cosmochimica Acta* 71:387–402.

Jourdan F., Renne P. R., and Reimold W. U. 2007. The problem of inherited Ar-40* in dating impact glass by the Ar-40/Ar-39 method: Evidence from the Tswaing impact crater (South Africa). *Geochimica et Cosmochimica Acta* 71:1214–1231.

Jourdan F., Renne P. R., and Reimold W. U. 2009. An appraisal of the ages of terrestrial impact structures. *Earth and Planetary Science Letters* 286:1–13.

Jourdan F., Moynier F., Koeberl C., and Eroglu S. 2011. $^{40}Ar/^{39}Ar$ age of the Lonar crater and consequence for the geochronology of planetary impacts. *Geology* 39:671–674.

Jourdan F., Reimold W. U., and Deutsch A. 2012. Dating terrestrial impact structures. *Elements* 8:49–53.

Jourdan F., Timms N. E., Eroglu E., Mayers C., Frew A., Bland P., Collins G., Davison T., Abe M., and Yada T. 2017. Collisional history of asteroid Itokawa. *Geology* 45:819–822.

Koeberl C., Bottomley R., Glass B. P., and Storzer D. 1997. Geochemistry and age of Ivory Coast tektites and microtektites. *Geochimica et Cosmochimica Acta* 61:1745–1772.

Koppers A. A. P. 2002. ArArCALC—Software for Ar-40/Ar-39 age calculations. *Computers & Geosciences* 28:605–619.

Lee J. Y., Marti K., Severinghaus J. P., Kawamura K., Yoo H. S., Lee J. B., and Kim J. S. 2006. A redetermination of the isotopic abundances of atmospheric Ar. *Geochimica et Cosmochimica Acta* 70:4507–4512.

Lee Y. T., Chen J. C., Ho K. S., and Juang W. S. 2004. Geochemical studies of tektites from East Asia. *Geochemical Journal* 38:1–17.

Lo C. H., Howard K. T., Chung S. L., and Meffre S. 2002. Laser fusion argon-40/argon-39 ages of Darwin impact glass. *Meteoritics & Planetary Science* 37:1555–1562.

Macris C. A., Asimow P. D., Badro J., Eiler J. M., Zhang Y., and Stolper E. M. 2018. Seconds after impact: Insights into the thermal history of impact ejecta from diffusion between lechatelierite and host glass in tektites and experiments. *Geochimica et Cosmochimica Acta* 241:69–94.

Mark D. F., Lindgren P., and Fallick A. 2014. A high-precision $^{40}Ar/^{39}Ar$ age for hydrated impact glass from the Dellen impact, Sweden. *Geological Society, London, Special Publications* 378:349–366.

Mark D. F., Renne P. R., Dymock R., Smith V. C., Simon J. I., Morgan L. E., Staff R. A., and Ellis B. S. 2017. High-precision $^{40}Ar/^{39}Ar$ dating of Pleistocene tuffs and temporal anchoring of the Matuyama-Brunhes boundary. *Quaternary Geochronology* 39:1–23.

McDougall I. and Harrison T. M. 1999. *Geochronology and thermochronology by the $^{40}Ar/^{39}Ar$ method*. Oxford: Oxford University Press. 269 p.

McDougall I. and Lovering J. 1969. Apparent K/Ar dates on cores and excess Ar in flanges of australites. *Geochimica et Cosmochimica Acta* 33:1057–1070.

Mizera J., Řanda Z., and Kameník J. 2016. On a possible parent crater for Australasian tektites: Geochemical, isotopic, geographical and other constraints. *Earth Science Reviews* 154:123–137.

Moynier F., Beck P., Jourdan F., Yin Q. Z., Reimold U., and Koeberl C. 2009. Isotopic fractionation of zinc in tektites. *Earth and Planetary Science Letters* 277:482–489.

Moynier F., Koeberl C., Beck P., Jourdan F., and Telouk P. 2010. Isotopic fractionation of Cu in tektites. *Geochimica et Cosmochimica Acta* 74:799–807.

Niespolo E. M., Rutte D., Deino A. L., and Renne P. R. 2017. Intercalibration and age of the Alder Creek sanidine $^{40}Ar/^{39}Ar$ standard. *Quaternary Geochronology* 39:205–213.

Nomade S., Renne P., Vogel N., Deino A., Sharp W., Becker T., Jaouni A., and Mundil R. 2005. Alder Creek sanidine (ACs-2): A Quaternary $^{40}Ar/^{39}Ar$ dating standard tied to the Cobb Mountain geomagnetic event. *Chemical Geology* 218:315–338.

Nomade S., Gauthier A., Guillou H., and Pastre J.-F. 2010. $^{40}Ar/^{39}Ar$ temporal framework for the Alleret maar lacustrine sequence (French Massif-Central): Volcanological and paleoclimatic implications. *Quaternary Geochronology* 5:20–27.

Nowak M., Schreen D., and Spickenbom K. 2004. Argon and CO_2 on the race track in silicate melts: A tool for the development of a CO, speciation and diffusion model. *Geochimica et Cosmochimica Acta* 68:5127–5138.

Renne P. R., Mundil R., Balco G., Min K. W., and Ludwig K. R. 2010. Joint determination of K-40 decay constants and Ar-40*/K-40 for the Fish Canyon sanidine standard, and improved accuracy for Ar-40/Ar-39 geochronology. *Geochimica et Cosmochimica Acta* 74:5349–5367.

Renne P. R., Balco G., Ludwig K. R., Mundil R., and Min K.. 2011. Response to the comment by W.H. Schwarz et al. on "Joint determination of K-40 decay constants and Ar-40*/K-40 for the Fish Canyon sanidine standard, and improved accuracy for Ar-40/Ar-39 geochronology" by PR Renne et al. (2010). *Geochimica et Cosmochimica Acta* 75: 5097–5100.

Renne P. R., Deino A. L., Hilgen F. J., Kuiper K. F., Mark D. F., Mitchell W. S., Morgan L. E., Mundil R., and Smit J. 2013. Time scales of critical events around the Cretaceous-Paleogene boundary. *Science* 339:684–687.

Roddick J. 1983. High precision intercalibration of 40Ar-39Ar standards. *Geochimica et Cosmochimica Acta* 47:887–898.

Schmieder M. and Jourdan F. 2013. The Lappajärvi impact structure (Finland): Age, duration of crater cooling, and implications for early life. *Geochimica et Cosmochimica Acta* 112:321–339.

Schmieder M., Jourdan F., Tohver E., and Cloutis E. A. 2014. $^{40}Ar/^{39}Ar$ age of the Lake Saint Martin impact structure (Canada)–Unchaining the Late Triassic terrestrial impact craters. *Earth and Planetary Science Letters* 406:37–48.

Schmieder M., Kennedy T., Jourdan F., Buchner E., and Reimold W. U. 2018. A high-precision $^{40}Ar/^{39}Ar$ age for the Nördlinger Ries impact crater, Germany, and implications for the accurate dating of terrestrial impact events. *Geochimica et Cosmochimica Acta* 220:146–157.

Schultze D., Hetch L., Jourdan F., Reimold W. U., and Schmitt R. T. 2016. Tenoumer impact crater, Mauretania: Impact melt genesis from a lithologically diverse target. *Meteoritics & Planetary Science* 51:323–350.

Schwarz W. H., Trieloff M., Bollinger K., Gantert N., Fernandes V. A., Meyer H. P., Povenmire H., Jessberger E. K., Guglielmino M., and Koeberl C. 2016. Coeval ages of Australasian, Central American and Western Canadian tektites reveal multiple impacts 790 ka ago. *Geochimica et Cosmochimica Acta* 178:307–319.

Spell T. L. and McDougall I. 2003. Characterization and calibration of $^{40}Ar/^{39}Ar$ dating standards. *Chemical Geology* 198:189–211.

Stöffler D., Artemieva N. A., and Pierazzo E. 2002. Modeling the Ries-Steinheim impact event and the formation of the moldavite strewn field. *Meteoritics & Planetary Science* 37:1893–1907.

Timms N. E., Erickson T. M., Zanetti M. R., Pearce M. A., Cayron C., Cavosie A. J., Reddy S. M., Wittmann A., and Carpenter P. K. 2017. Cubic zirconia in >2370 °C impact melt records Earth's hottest crust. *Earth and Planetary Science Letters* 477:52–58.

Valet J.-P., Bassinot F., Bouilloux A., Bourlès D., Nomade S., Guillou V., Lopes F., Thouveny N., and Dewilde F. 2014. Geomagnetic, cosmogenic and climatic changes across the last geomagnetic reversal from Equatorial Indian Ocean sediments. *Earth and Planetary Science Letters* 397:67–79.

Yamei H., Potts R., Baoyin Y., Zhengtang G., Deino A., Wei W., Clark J., Guangmao X., and Weiwen H. 2000. Mid-Pleistocene Acheulean-like stone technology of the Bose basin, South China. *Science* 287:1622–1626.

Zhang Y., Xu Z., Zhu M., and Wang H. 2007. Silicate melt properties and volcanic eruptions. *Reviews of Geophysics* 45:2006RG000216.

SUPPORTING INFORMATION

Additional supporting information may be found in the online version of this article:

Annex S1. Ar isotopic data corrected for blank, mass discrimination and radioactive decay for each analysis. Uncertainties on individual isotope abundances are given at the 1σ level.

Annex S2. $^{39}Ar/^{40}Ar$ vs. $^{36}Ar/^{40}Ar$ inverse isochron plots obtained at Curtin University with an ARGUS VI multicollector and a MAP 250-50 single collector instrument for a total of five aliquots from four tektites (Chinese, Thai, Vietnamese, and Western Australia). Ages are quoted at the 2σ level.

Annex S3. $^{39}Ar/^{40}Ar$ vs. $^{36}Ar/^{40}Ar$ inverse isochron plots obtained at the LSCE laboratory (Gif) with a VG5400 single-collector for three tektites (Chinese, Thai, and Vietnamese samples). Ages are quoted at the 2σ level.